

Motion of polar cap patches: A statistical study with all-sky airglow imager at Resolute Bay, Canada

K. Hosokawa,¹ T. Kashimoto,¹ S. Suzuki,² K. Shiokawa,³ Y. Otsuka,³ and T. Ogawa⁴

Received 25 December 2008; revised 12 February 2009; accepted 6 March 2009; published 25 April 2009.

[1] A highly sensitive all-sky airglow imager (part of the Optical Mesosphere Thermosphere Imagers [OMTIs]) has been operating for 3 years at Resolute Bay, Canada (geographic latitude 74.7°N; geomagnetic latitude 82.9°N) since January 2005. One of its major applications is the observation of polar cap patches. Polar cap patches are generated in the vicinity of the cusp during southward interplanetary magnetic field (IMF) conditions, and they exhibit dynamic movement, possibly in association with the changes in the IMF orientation. In order to determine how their motions are controlled by the upstream IMF conditions, we applied a motion-tracking algorithm that was based on two-dimensional cross-correlation analysis to consecutive images obtained from January 2005 to December 2007 by the all-sky airglow imager at Resolute Bay. We identified and extracted 561 individual patches and then carried out a statistical study of their motion. It is demonstrated that the speed of patches is primarily controlled by the IMF B_z . Furthermore, the dawn-dusk component of the patch drift velocities is well correlated with the IMF B_y , which is in good agreement with the published B_y dependence of the nightside polar cap convection. This enables us to monitor the plasma convection within the polar cap by using polar cap patches as tracers.

Citation: Hosokawa, K., T. Kashimoto, S. Suzuki, K. Shiokawa, Y. Otsuka, and T. Ogawa (2009), Motion of polar cap patches: A statistical study with all-sky airglow imager at Resolute Bay, Canada, *J. Geophys. Res.*, *114*, A04318, doi:10.1029/2008JA014020.

1. Introduction

[2] Polar cap patches, which are regions of plasma density enhancement in the polar cap F region ionosphere, are generated in the vicinity of the dayside cusp during southward interplanetary magnetic field (IMF) conditions. The plasma density within the polar cap patches is often enhanced by a factor of 2–10 above a background level [Weber *et al.*, 1984]. After initiation, they are transported toward the nightside across the polar cap along the streamlines of high-latitude plasma convection [Crowley, 1996]. The dynamical characteristics of polar cap patches have been investigated using all-sky airglow imager [Weber *et al.*, 1984, 1986], coherent HF radar [Ogawa *et al.*, 1998; Milan *et al.*, 2002], incoherent scatter radar [Pedersen *et al.*, 1998, 2000], and ionosonde [MacDougall and Jayachandran, 2007]. To date, however, no study has examined the motion of patches in a statistical manner. A major obstacle to conducting such research is the difficulty involved in

automatically computing the motion of patches from a large data set.

[3] Recently, Hosokawa *et al.* [2006] developed an algorithm for estimating the motion of polar cap patches from 630.0 nm all-sky images obtained by an all-sky imager at Resolute Bay, Canada. This algorithm is based on two-dimensional cross-correlation analysis of consecutive airglow images. By using this algorithm, it is possible to derive the speed and direction of motion of patches within the field of view (FOV) with a temporal resolution of 2 min. Hosokawa *et al.* demonstrated, through case example, that polar cap patches change their speed and direction in correlation with the upstream IMF orientation; that is, the speed of patches is primarily controlled by the IMF B_z component and the direction of their drift velocities are well correlated with the IMF B_y component.

[4] In this study, we extend the work of Hosokawa *et al.* [2006] by applying their method to all available all-sky images recorded for three years at Resolute Bay. The speed and direction of patch motion are examined statistically, and their dependence on the upstream IMF orientations is discussed in terms of the variations in the polar cap plasma convection through the magnetosphere-ionosphere coupling process.

2. Instrumentation

[5] An all-sky airglow imager has been operational at Resolute Bay, Canada (74.73°N, 265.07°E; AACGM latitude 82.9°) since January 2005 [Hosokawa *et al.*, 2006,

¹Department of Information and Communication Engineering, University of Electro-Communications, Chofu, Tokyo, Japan.

²Sugadaira Space Radio Observatory, University of Electro-Communications, Chofu, Tokyo, Japan.

³Solar-Terrestrial Environment Laboratory, Nagoya University, Nagoya, Japan.

⁴National Institute of Information and Communications Technology, Koganei, Tokyo, Japan.

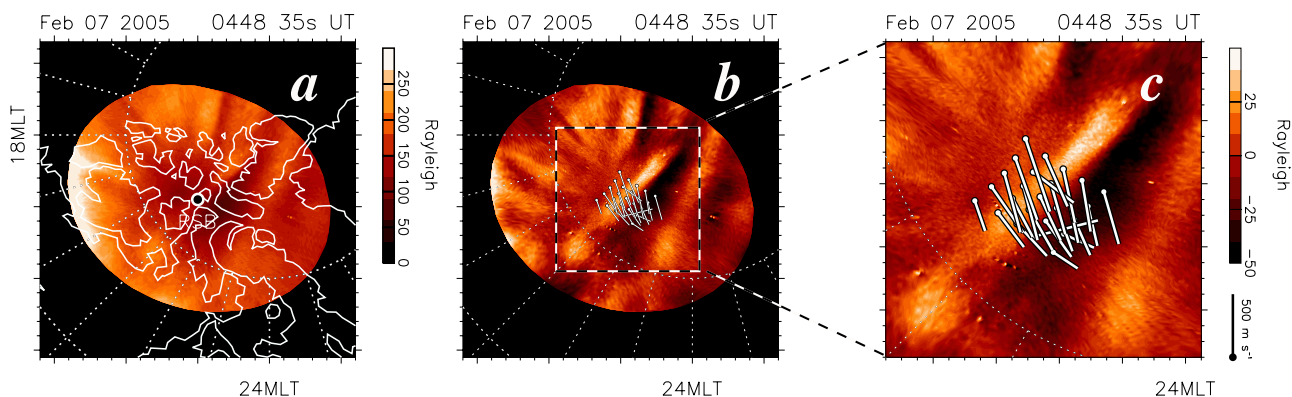


Figure 1. (a) Image of an all-sky 630 nm airglow observation of polar cap patches at 0448 UT on 7 February 2005 at Resolute Bay, Canada. The image is mapped in MLT/magnetic latitude coordinates, and the absolute airglow intensity is displayed in units of Rayleigh. Magnetic noon is to the top, and the dotted circles represent magnetic latitudes of 70° and 80° , respectively. The field of view of the imager is mapped assuming that the height of optical emission is 250 km. (b) Same image as in Figure 1a but with deviations from 1-hour running average plotted to indicate weak perturbations in airglow intensity associated with the patches. (c) Zoomed view of the center of the field of view of the imager on which the estimated patch motion vectors are overlotted.

2009] as part of the Optical Mesosphere Thermosphere Imagers (OMTIs) [Shiokawa *et al.*, 1999, 2009]. The imager has a number of optical filters for the 557.7 nm, 630.0 nm, 777.4 nm, Na-line and OH-band airglow emissions. In the present analysis, all-sky airglow images at a wavelength of 630.0 nm (OI, emission altitude ranges from 200 to 300 km), which are obtained every 2 min with an exposure time of 30 s, are employed for determining the motion of polar cap patches. Additionally, time series of the optical intensities at wavelengths of 630.0 nm and 577.7 nm measured at the zenith are used for the automated extraction of patch appearance. The background continuum emission from the sky is sampled every 20 min at a wavelength of 572.5 nm, and it is used to compute the absolute intensity of the airglow lines [Shiokawa *et al.*, 2000, 2009]. The imager is operational from September to March, when the Sun and the Moon are sufficiently below the horizon. The data of three years, from January 2005 to December 2007, are statistically analyzed in the current study.

3. Methodology

[6] Figure 1a shows an example of a 630.0 nm airglow image obtained at 0448 UT on 7 February 2005. The raw all-sky image was converted into the altitude adjusted corrected geomagnetic (AACGM) coordinates [Baker and Wing, 1989] assuming an emission height of 250 km and then mapped into coordinates of magnetic local time (MLT) and magnetic latitude. Magnetic midnight is to the bottom, and the dotted circles represent magnetic latitudes of 70° and 80° , respectively. Here, the absolute optical intensities are displayed in units of Rayleigh. A few bright structures extending mainly in the south–north direction are observed in the poleward part of the FOV. These observed structures are a manifestation of the polar cap patches in the optical data. It should be noted that the more prominent feature in the equatorward part of the FOV does not correspond to patches, but it is the poleward edge of the auroral oval. To investigate

weaker airglow enhancement caused by the patches, deviations from 1-hour running averages are displayed in units of Rayleigh in Figure 1b, where the velocity vectors of the patches as estimated by the method of Hosokawa *et al.* [2006] are superimposed. Figure 1c concentrates on the central part of the FOV (indicated by the dashed rectangle in Figure 1b). It is clearly seen that a patch extending from south to north (see meridian directions shown in Figure 1a) is located near the zenith in the FOV. The estimated patch velocities are directed eastward, that is, they are almost perpendicular to the alignment of the patch. The sequence of all-sky images during this interval (not shown) demonstrates that the estimated motion vectors trace the actual motion of patches very accurately.

[7] As mentioned previously, the method of Hosokawa *et al.* [2006] tracks the motion of polar cap patches quite well. However, it is important to note that since cross-correlation analysis is based on the optical data that is obtained in the vicinity of the zenith, the derived motion vectors cannot represent an actual motion of patches unless they are at the zenith. In such a case, the derived vectors cannot be used in the current statistical analysis. During extended intervals of southward IMF B_z , polar cap patches dominate the polar cap region and are observed almost continuously with the all-sky imager. However, when the IMF B_z is directed northward, sun-aligned arcs, the other prominent phenomenon occurring in the polar cap region, dominate the polar cap [Valladares *et al.*, 1994]. The purpose of this study is to examine the motion of polar cap patches. Thus it is necessary to first distinguish patches from sun-aligned arcs and to then process the obtained velocities of the patches when they are located around the zenith. For this purpose, we developed a method for automatically detecting the occurrence of polar cap patches from the time series of optical data obtained at the zenith.

[8] Figure 2 describes how the occurrence of patches at the zenith can be detected by this method. The interval considered here is between 0100 and 0600 UT on 7 February

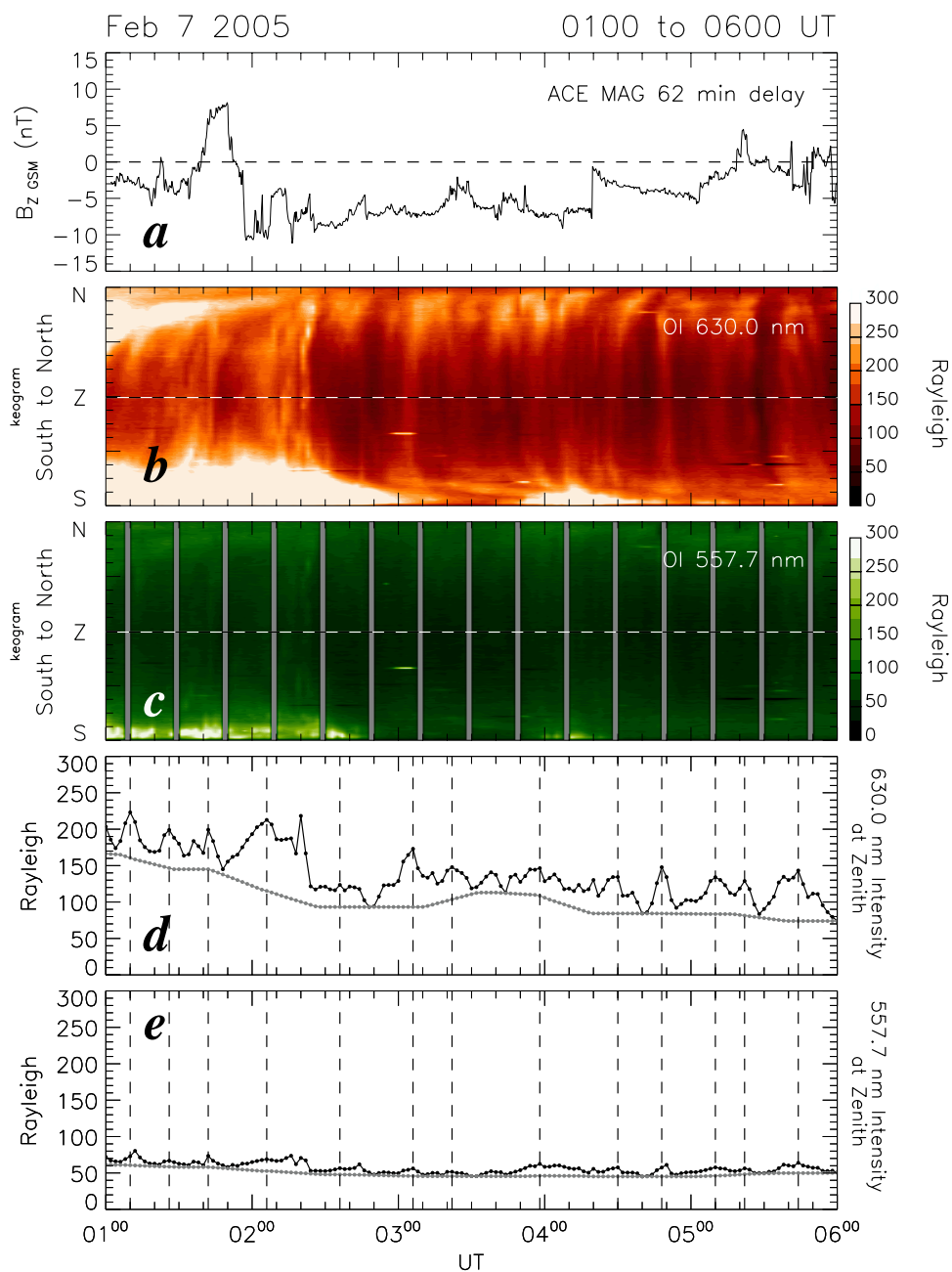


Figure 2. (a) IMF B_z components measured by the ACE spacecraft and time shifted by 62 min to allow for solar wind propagation delay. (b) North-South keograms of 630.0 nm all-sky images. (c) North-South keograms of 557.7 nm all-sky images. The horizontal dashed line indicates the zenith of the all-sky imager. (d) Time series of 630.0 nm emission intensity at the zenith of the all-sky camera. (e) Time series of 557.7 nm emission intensity at the zenith of the all-sky camera. The vertical dashed lines mark the times when the centers of polar cap patches are located at the zenith.

2005. Figure 2a shows the IMF B_z as monitored by the ACE spacecraft located upstream of the Earth ($X_{gsm} = 219.7 R_E$). A solar wind velocity of $\approx 420 \text{ km s}^{-1}$ was measured by ACE, corresponding to a delay of 60 min between the observed IMF feature and its incidence on the dayside magnetopause. An additional 2 min must be added to account for the propagation of Alfvén waves from the subsolar magnetopause to the dayside polar cap ionosphere. These calculations are based on the technique developed by *Khan and Cowley* [1999]. The time series of the IMF B_z was

shifted accordingly. Except for brief excursions to positive values at around 0140 UT, 0520 UT, and 0550 UT, the IMF B_z was predominantly negative; this condition is favorable for the formation of polar patches near the dayside cusp and their transport toward the central polar cap region.

[9] Figures 2b and 2c show the south–north keograms created from 630.0 nm and 577.7 nm airglow images, respectively. The horizontal dashed line corresponds to the zenith. Here, the absolute optical intensities are displayed in units of Rayleigh. Note that the observation at 557.7 nm is

absent every 20 min because the background continuum emission (572.5 nm) has to be sampled at these times in order to derive the absolute optical intensity. The instances of absent 557.7 nm observations are masked with gray lines in Figure 2c. A number of patches can be observed as slanted bright traces in the keogram of 630.0 nm. The continuous luminous structure observed in the southern part of the keogram between 0100 UT and 0300 UT corresponds to the daytime dense plasma, which is still illuminated by the sun from under the horizon, since the terminator at F region altitudes is substantially offset from that at the ground level. Throughout this interval, patches appeared from the south (i.e., from the daytime sunlit region) and drifted northward; this demonstrates that the patches drifted antisunward. It is important to note that there is no apparent indication of polar patches in the 557.7 nm keogram. Since polar cap patches are basically F region phenomena, the optical intensities within patches are significantly weaker at 557.7 nm than that at 630.0 nm. In contrast, polar cap aurorae (also known as sun-aligned arcs) [Valladares *et al.*, 1994] are observed much more prominently at both wavelengths. This difference enables us to distinguish between the patches and sun-aligned arcs by comparing the optical intensities of 557.7 nm and 630.0 nm emissions.

[10] Figures 2d and 2e show the time series of 630.0 nm and 557.7 nm emission intensities, respectively, measured at the zenith as a black line with dots. The data gaps in 557.7 nm observations, which occurred every 20 min, are linearly interpolated in the time series. The superimposed gray line with dots indicates a baseline estimated by smoothing the local minimums within a 1-hour running window, which represents a possible diurnal variation in the airglow intensity. To identify and extract instances of patch occurrence, we search the data points in the time series sequentially. During this sequential examination, we define a search window of duration 12 min surrounding the data point currently being considered. Then, we select the data point as an instance of patch occurrence if all the following conditions are satisfied: (1) the 630.0 nm emission intensity at the current data point should be the highest within the window, (2) the 630.0 nm emission intensity should be higher than the baseline by 30 R, and (3) the 557.7 nm emission intensity should not be higher than the baseline by 20 R. In addition to these criteria, we checked the sky conditions every 1 hour and only considered the data obtained in good weather conditions. The patches that were detected using this procedure are indicated by vertical dashed lines in Figures 2d and 2e. Thirteen individual patches were detected in this interval, most of which had a clear counterpart in the keograms shown in Figure 2b. However, the number of patches listed is likely to be slightly less than the number of patch signatures seen in Figure 2b. For example, the large peak seen around 0220 UT was not detected by the current algorithm, even though it was actually the signature of a polar cap patch traversing the zenith at Resolute Bay. This is mainly due to the employment of selection criteria 2 and 3. These criteria were employed for preventing faint sun-aligned arcs, whose emissions are prominent in both 557.7 nm and 630.0 nm observations, from being identified as patches. In the absence of these two criteria, the number of the detected patches would have been double. However, incorrect iden-

tification of sun-aligned arcs as patches would have considerably contaminated the statistical results; therefore, we processed the data using these selection criteria. Another incorrect identification occurred at around 0237 UT. In this case, the algorithm selected a very small peak whose optical intensity at 630 nm was 30 R above the background level. However, it had no corresponding trace in the 630 nm keogram. This inconsistency suggests that the list of polar cap patches considered in the current study does contain some unreliable peaks. We checked the other intervals and found that 5–10% of the events in the list were not associated with a significant peak in the 630 nm keogram, which demonstrates the limitations of the algorithm. We applied this procedure to all available optical observations at Resolute Bay from January 2005 to December 2007. Consequently, 561 individual patches were identified in total.

4. Motion of Polar Cap Patches

[11] For the 561 individual polar cap patches extracted in the previous section, their moving velocities estimated by the method of Hosokawa *et al.* [2006] were examined statistically. In particular, the relationship between the patch velocities and the upstream IMF orientations is discussed in detail. To compare the patch velocities with the IMF parameters, we used the 1 min high-resolution OMNI data (<http://omniweb.gsfc.nasa.gov>) to obtain the IMF values at the bow shock; an additional time shift of 10 min was considered to account for the delay from the bow shock to the polar cap ionosphere. Furthermore, since the characteristics of the patches change at a slow pace (in other words the patch stays for at least 10 min around the zenith), our velocity estimation with a temporal resolution of 2 min would introduce multiple velocity data for a single patch. Thus we considered all the velocity data within the 12 min search window around the time when the patch was located exactly at the zenith. This procedure can increase the number of data points in the statistics and would hence increase the significance of the statistical distributions.

[12] Figure 3a shows an occurrence distribution of patches as a function of their speed. The distribution is fairly symmetric, with the maximum occurrence of patches found at speeds around 300 m s^{-1} . It should be noted that patch speeds higher than 500 m s^{-1} were rare. Statistics of polar cap convection by using the Canadian Digital Ionosonde (CADI) measurements at Resolute Bay by MacDougall and Jayachandran [2001] showed that convection speeds lower than 500 m s^{-1} are dominant in the central polar cap region. However, convection speeds higher than 500 m s^{-1} can be observed to some extent. One of the major differences between the Digisonde measurements by MacDougall and Jayachandran and our measurements derived from optical observations is that our optical instrument could be operated only during nighttime. The spatial relationship of the geographic and geomagnetic poles, in particular, prevented us from observing the dayside part of the polar cap with the all-sky imager at Resolute Bay. Generally, polar cap convection speed is higher on the dayside than on the nightside; this can be seen in the high-latitude plasma convection models such as those developed by Weimer [1995] and Ruohoniemi and

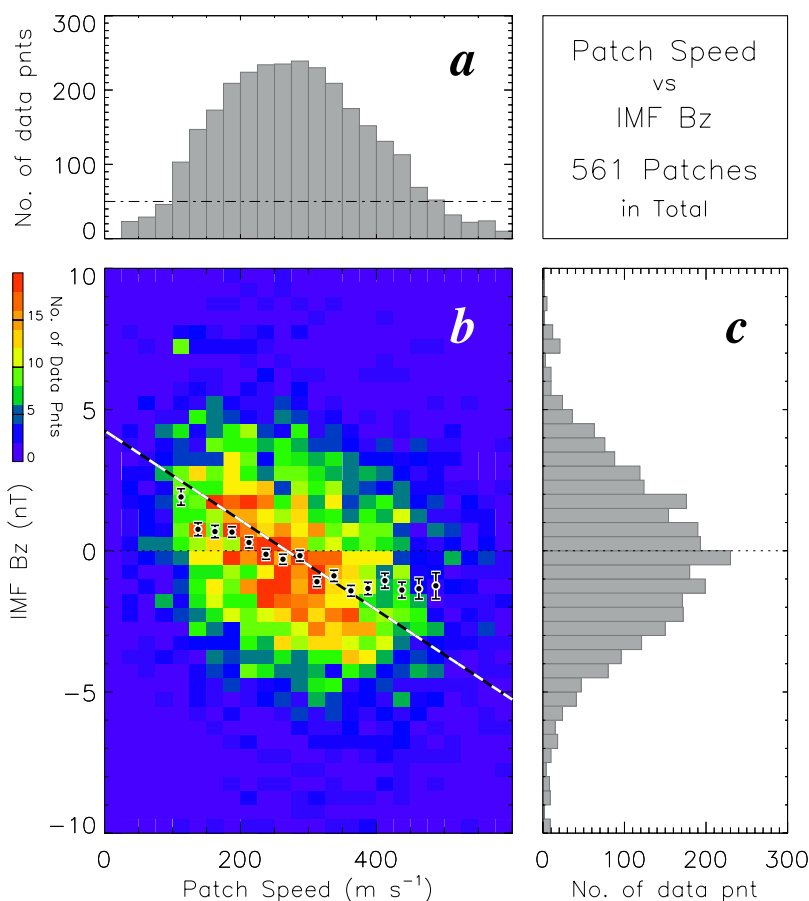


Figure 3. (a) Occurrence distribution of moving speed of patches. (b) Distribution of the speed of patches as a function of the IMF B_z . The density of data points is self-normalized and shown on a linear scale. The dots and bars represent the mean and standard error of the distributions, respectively, in 25 m s^{-1} wide bins of patch speed. (c) Occurrence distribution of the IMF B_z at instances of patch detection at Resolute Bay.

Greenwald [2005]. Thus the local time coverage of the optical observation could result in fewer high-speed patches in our statistical result. Another possible reason for fewer high-speed patches in our statistical analysis is that we used the data obtained during the recent solar minimum (2005 to 2007), when the magnitude of the IMF was typically smaller than that during the solar maximum. This tendency can be seen in Figure 3c, which shows the occurrence distribution of the IMF B_z . The magnitude of the IMF B_z was mostly below 5 nT. In such a situation, we cannot expect the IMF to drive the polar cap convection severely and consequently, the occurrence of high-speed patches would be less frequent.

[13] Figure 3b shows the distribution of patch speed as a function of the IMF B_z . The dots and bars indicate the mean of the distribution and standard error of the mean (σ/\sqrt{N} , where σ is the standard deviation and N is the number of data points, respectively) in 25 m s^{-1} wide bins of patch speed. In order to discard the data of low statistical significance, the mean and standard error are displayed only if the number of data points in the bin is greater than 50 (marked by the dash-dotted line in Figure 3a). In general, the patch speed was higher for more negative values of IMF B_z . This overall trend is consistent with a number of past

studies that showed that the polar cap convection speed increases when the IMF B_z becomes more southward. For example, *MacDougall and Jayachandran* [2001] demonstrated that the general relationship between the IMF B_z and speed of polar cap convection at Resolute Bay can be expressed as $V (\text{m s}^{-1}) = 268 - 63 B_z (\text{nT})$ for an interval of $B_z > -10 \text{ nT}$, which is overplotted as the dashed line in Figure 3b. The mean of the distribution as estimated by the current statistics and the model of *MacDougall and Jayachandran* [2001] (dashed line) are roughly consistent with each other; this strongly suggests that the speeds of the patches shown here are in good agreement with the polar cap plasma convection speeds obtained by other observational techniques. However, some offset can be observed between the two distributions at speeds higher than 400 m s^{-1} . The reason for this is unknown at the moment. However, the statistical significance in our case might not be sufficient, because the number of data points considered in the statistics is small and the standard error of the distribution is relatively large, in this area.

[14] Figure 3c shows an occurrence distribution of the IMF B_z at instances when patches were detected over Resolute Bay. Interestingly, it was found that patches occurred even during intervals of northward IMF. *Oksavik*

et al. [2006] introduced a case in which patches were formed due to soft particle precipitation inside a lobe cell during northward IMF conditions. However, most past studies have suggested that patches are normally generated during southward IMF conditions, which contradicts the current result. It should be noted that we observed patches mostly on the nightside, at least 1000 km away from the possible source of patches near the dayside cusp. Since it takes approximately 1 hour for patches to travel from their source to the point of observations, assuming the average speed of patches to be 300 m s^{-1} , it is possible that even if patches were generated in the source region near the dayside cusp during a southward IMF condition, the polarity of the IMF could change during the time the patches took to travel to Resolute Bay. To confirm this hypothesis, we are now trying to back trace the optical patches observed in the central polar cap (i.e., at Resolute Bay) to the dayside cusp inflow region using the convection velocity data derived using the SuperDARN map-potential technique [Ruohoniemi and Baker, 1998]. This will enable us to verify the polarity of the IMF B_z at the time of patch generation.

[15] Another possible explanation for the detection of patches during positive IMF B_z conditions could be that the patches are in fact generated during northward IMF conditions. There have been several mechanisms proposed for explaining the generation of patches. A majority of past studies considered that the temporal variation of plasma convection near the dayside cusp entrains the dayside dense plasma into the polar cap, forming a patch. However, a recent paper by MacDougall and Jayachandran [2007] explained the patch generation by low-energy precipitation into the returning flow from the nightside to the dayside around the dawn convection cell. Lockwood and Carlson [1992] have suggested that a time-varying reconnection rate or the transient occurrence of flux transfer events (FTEs [Russell and Elphic, 1978]) could act as a generation mechanism. It has also been suggested that the electron density depletion between patches could arise due to rapid plasma drift in short-lived flow channels located near the cusp region, resulting in enhanced ion-frictional or Joule heating, which in turn increases the plasma recombination rate [Rodger *et al.*, 1994; Ogawa *et al.*, 2001]. These flow channels are produced by FTEs, and hence this mechanism is also associated with transient reconnection. McWilliams *et al.* [2000] investigated the occurrence distribution of pulsed ionospheric flows event, which are a signature of FTEs in the dayside ionosphere, in a statistical manner. They demonstrated that 33% of the events occurred during northward IMF conditions. This suggests that the temporal variation of the ionospheric plasma flow is available for generating patches even when the IMF B_z is positive. The existence of patches in the central polar cap during the interval of positive IMF B_z allows us to study the plasma convection in the polar cap region by using patches as tracers even when the IMF is directed northward. This makes it possible to monitor the motion of plasma in the polar cap region in a more continuous manner.

[16] We now discuss the relationship between the direction of patch motion and the east-west component of the IMF. A number of statistical studies on high-latitude plasma convections have been conducted using radar [Ruohoniemi and Greenwald, 1996, 2005] and polar-orbiting satellite

measurements [Weimer, 1995]. These studies showed that the nightside polar cap flow is directed from dawn (dusk) to dusk (dawn) for the positive (negative) B_y conditions. Figure 4b presents an occurrence distribution of the direction of patch motion as a function of the IMF B_y . Here, we consider the azimuth of the patch's moving velocity relative to the noon-midnight line (hereinafter we call this parameter as θ) as a proxy for the direction of the patches. A positive (negative) θ corresponds to a drift velocity directed toward dusk (dawn). The dots and bars show the mean of the distributions and standard error of the mean, respectively, in 5° wide bins of θ . As mentioned previously, the mean and standard error are displayed only if the number of data points in the bin (shown in Figure 4a) is greater than 50, in order to exclude data of less statistical significance. It is demonstrated that the θ becomes positive (negative), corresponding to drift velocity directed toward dusk (dawn), when the IMF B_y is positive (negative). In other words, the drift direction of the patches is controlled by the polarity of the IMF B_y . This is in good agreement with the published B_y dependence of the nightside polar cap convection.

[17] A noteworthy feature of Figure 4b is that the distribution is not symmetrical about the line indicating IMF $B_y = 0$. If the twin-cell convection pattern is completely symmetrical about the noon-midnight line, then θ should be 0° when the magnitude of the IMF B_y component is close to 0 nT. In reality, however, θ is approximately 20° when the IMF B_y magnitude is 0 nT. This indicates that the polar cap convection rotates approximately 20° clockwise from symmetry, even in the interval where IMF $B_y \approx 0$. This tendency can be identified in all previous high-latitude convection models [Ruohoniemi and Greenwald, 2005 and references therein] and in the results of numerical magnetohydrodynamic (MHD) simulation [Tanaka, 2001]. In the convection model based on data from the SuperDARN Goose Bay radar [Ruohoniemi and Greenwald, 1996], we can see that the convection streamlines at polar cap latitudes actually rotate about 20° clockwise from the symmetric twin-cell pattern [e.g., see Ruohoniemi and Greenwald, 1996, Figure 7], irrespective of the sign of the IMF B_z . A mechanism explaining the breakdown of the mirror symmetry due to the effect of day-night conductivity gradient in the polar cap region was originally proposed by Atkinson and Hutchison [1978]. This mechanism works as follows: If we assume a sharp day-night conductivity gradient across the polar cap, the primary Hall currents, flowing from midnight to noon, are interrupted by the change in conductivity at the terminator. In order to satisfy current continuity, the electric field is modified to include a secondary component that is oriented toward the terminator on either side of it. As a result, the antisunward flow in the polar cap is modified, and this breaks the mirror symmetry with respect to the IMF B_y .

[18] The current statistical results confirmed that polar cap patches were transported strictly along the streamlines of the polar cap convection. On the basis of this result, we can use polar cap patches as tracers for observing polar cap convection. As shown in Figure 2, polar cap patches were observed almost continuously during an extended interval of the IMF B_z , indicating that continuous monitoring of polar cap convection is possible by optical observation at Resolute Bay. Continuous monitoring of ionospheric con-

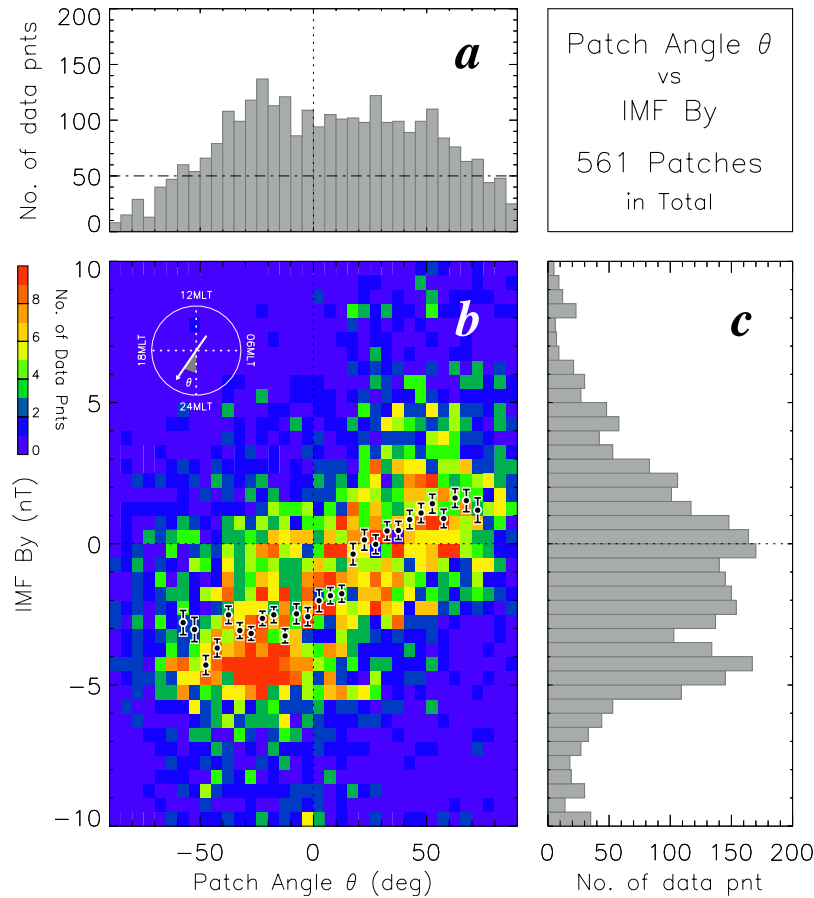


Figure 4. (a) Occurrence distribution of moving direction of patches (θ : angle of azimuth relative to the noon-midnight line). (b) Distribution of θ as a function of the IMF B_y . The density of data points is self-normalized and shown on a linear scale. The dots and bars represent the mean and standard error of the distributions, respectively, in 5° wide bins of patch speed. (c) Occurrence distribution of the IMF B_y when patches are observed at Resolute Bay.

vection during a substorm cycle is very important for studying the auroral breakup process. Under the framework of the THEMIS mission, five spacecraft cover the Canadian longitudinal sector, where Resolute Bay is located, and extensive studies on substorm processes are being conducted by combining various ground-based and space-based observations. The polar cap convection database derived using the current method could be quite useful for collaborative ground-based and satellite studies of substorms in the near future.

5. Summary and Conclusion

[19] We conducted, for the first time, a statistical analysis of the motion of polar cap patches by using the large data set of observations obtained by the all-sky airglow imager located in the polar cap region at Resolute Bay, Canada. We identified 561 individual patches with 630.0 nm and 557.7 nm airglow emissions by using an automated detection algorithm. Statistical results show that the speed of patch motion was almost linearly correlated with the magnitude of the southward component of the IMF. Quantitatively, the results are in good agreement with the statistical formula proposed by *MacDougall and Jayachandran*

[2001] based on CADI observations in the polar cap. The directions of the patch drift velocities were well correlated with the IMF B_y , which is in good agreement with the published B_y dependence of the nightside polar cap convection. Our statistics clearly demonstrate that the polar cap plasma convection is not symmetrical about the noon-midnight line even when the IMF B_y was ≈ 0 . This is also consistent with past models of the high-latitude convection pattern. The excellent overall agreement with the past observations and modeled results strongly suggests that the motion of the patches is strictly controlled by the upstream IMF orientations. This allows us to monitor polar cap convection by using optical patches as tracers.

[20] **Acknowledgments.** We thank Y. Katoh, M. Satoh, and T. Katoh of the Solar-Terrestrial Environment Laboratory (STEL), Nagoya University, for their kind support of airglow imaging observations. This work was supported by a Grant-in-Aid for Scientific Research (16403007, 19403010) of the Ministry of Education, Culture, Sports, Science and Technology of Japan, and the Project 2 of the Geospace Research Center, STEL. The authors wish to thank N. Ness at Bartol Research Institute for access to data from MFI and SWE instruments onboard the ACE spacecraft. Special thanks also go to the people in the Narwhal Arctic Service at Resolute Bay for their kind and helpful support in operating the optical instrument.

[21] Zuyin Pu thanks Marc Hairston and another reviewer for their assistance in evaluating this paper.

References

- Atkinson, G., and D. Hutchison (1978), Effect of the day night ionospheric conductivity gradient on polar cap convective flow, *J. Geophys. Res.*, **83**, 725.
- Baker, K. B., and S. Wing (1989), A new magnetic coordinate system for conjugate studies of high latitudes, *J. Geophys. Res.*, **94**, 9139.
- Crowley, G. (1996), Critical review of ionospheric patches and blobs, in *Review of Radio Science 1993–1996*, edited by W. R. Stone, p. 619, Oxford Univ. Press, New York.
- Hosokawa, K., K. Shiokawa, Y. Otsuka, A. Nakajima, T. Ogawa, and J. D. Kelly (2006), Estimating drift velocity of polar cap patches with all-sky airglow imager at Resolute Bay, Canada, *Geophys. Res. Lett.*, **33**, L15111, doi:10.1029/2006GL026916.
- Hosokawa, K., K. Shiokawa, Y. Otsuka, T. Ogawa, J.-P. St-Maurice, G. J. Sofko, and D. A. Andre (2009), The relationship between polar cap patches and field-aligned irregularities as observed with an all-sky airglow imager at Resolute Bay and the PolarDARN radar at Rankin Inlet, *J. Geophys. Res.*, **114**, A03306, doi:10.1029/2008JA013707.
- Khan, H., and S. W. H. Crowley (1999), Observations of the response time of high-latitude ionospheric convection to variations in the interplanetary magnetic field using EISCAT and IMP-8 data, *Ann. Geophys.*, **17**, 1306.
- Lockwood, M., and H. C. Carlson Jr. (1992), Production of polar cap electron density patches by transient magnetopause reconnection, *Geophys. Res. Lett.*, **19**, 1731.
- MacDougall, J. W., and P. T. Jayachandran (2001), Polar cap convection relationships with solar wind, *Radio Sci.*, **36**, 1869.
- MacDougall, J. W., and P. T. Jayachandran (2007), Polar patches: Auroral zone precipitation effects, *J. Geophys. Res.*, **112**, A05312, doi:10.1029/2006JA011930.
- McWilliams, K. A., T. K. Yeoman, and G. Provan (2000), A statistical survey of dayside pulsed ionospheric flows as seen by the CUTLASS Finland HF radar, *Ann. Geophys.*, **18**(4), 445–453.
- Milan, S. E., M. Lester, and T. K. Yeoman (2002), HF radar polar patch formation revisited: Summer and winter variations in dayside plasma structuring, *Ann. Geophys.*, **20**, 487.
- Ogawa, T., N. Nishitani, M. Pinnock, N. Sato, H. Yamagishi, and A. S. Yukimatu (1998), Antarctic HF radar observations of irregularities associated with polar patches and auroral blobs: A case study, *J. Geophys. Res.*, **103**, 26,547.
- Ogawa, T., S. C. Buchert, N. Nishitani, N. Sato, and M. Lester (2001), Plasma density suppression process around the cusp revealed by simultaneous CUTLASS and EISCAT Svalbard radar observations, *J. Geophys. Res.*, **106**, 5551.
- Oksavik, K., J. M. Ruohoniemi, R. A. Greenwald, J. B. H. Baker, J. Moen, H. C. Carlson, T. K. Yeoman, and M. Lester (2006), Observations of isolated polar cap patches by the European Incoherent Scatter (EISCAT) Svalbard and Super Dual Auroral Radar Network (SuperDARN) Finland radars, *J. Geophys. Res.*, **111**, A05310, doi:10.1029/2005JA011400.
- Pedersen, T., B. Fejer, R. Doe, and E. Weber (1998), Incoherent scatter radar observations of horizontal F region plasma structure over Sondrestrom, Greenland, during polar cap patch events, *Radio Sci.*, **33**, 1847.
- Pedersen, T., B. Fejer, R. Doe, and E. Weber (2000), An incoherent scatter radar technique for determining two-dimensional horizontal ionization structure in polar cap F region patches, *J. Geophys. Res.*, **105**, 10,637.
- Rodger, A. S., M. Pinnock, J. R. Dudeney, K. B. Baker, and R. A. Greenwald (1994), A new mechanism for polar patch formation, *J. Geophys. Res.*, **99**, 6425.
- Ruohoniemi, J. M., and K. B. Baker (1998), Response of high latitude convection to a sudden southward IMF turning, *Geophys. Res. Lett.*, **25**, 2913.
- Ruohoniemi, J. M., and R. A. Greenwald (1996), Statistical patterns of high-latitude convection obtained from Goose Bay HF radar observations, *J. Geophys. Res.*, **101**, 21,743.
- Ruohoniemi, J. M., and R. A. Greenwald (2005), Dependencies of high-latitude plasma convection: Consideration of interplanetary magnetic field, seasonal, and universal time factors in statistical patterns, *J. Geophys. Res.*, **110**, A09204, doi:10.1029/2004JA010815.
- Russell, C. T., and R. C. Elphic (1978), Initial ISEE magnetometer results: Magnetopause observations, *Space Sci. Rev.*, **22**, 681.
- Shiokawa, K., Y. Katoh, M. Satoh, M. K. Ejiri, T. Ogawa, T. Nakamura, T. Tsuda, and R. H. Wiens (1999), Development of optical mesosphere thermosphere imagers (OMTI), *Earth Planets Space*, **51**, 887.
- Shiokawa, K., Y. Katoh, M. Satoh, M. K. Ejiri, and T. Ogawa (2000), Integrating-sphere calibration of all-sky cameras for nightglow measurements, *Adv. Space Res.*, **26**, 1025.
- Shiokawa, K., Y. Otsuka, and T. Ogawa (2009), Propagation characteristics of nighttime mesospheric and thermospheric waves observed by optical mesosphere thermosphere imagers at middle and low latitudes, *Earth Planets Space*, in press.
- Tanaka, T. (2001), Interplanetary magnetic field By and auroral conductance effects on high-latitude ionospheric convection patterns, *J. Geophys. Res.*, **106**, 24,505.
- Valladares, C., H. Carlson Jr., and K. Fukui (1994), Interplanetary magnetic field dependency of stable sun-aligned polar cap arcs, *J. Geophys. Res.*, **99**, 6247.
- Weber, E. J., J. Buchau, J. G. Moore, J. R. Sharber, R. C. Livingston, J. D. Winningham, and B. W. Reinisch (1984), F layer ionization patches in the polar caps, *J. Geophys. Res.*, **89**, 1683.
- Weber, E. J., et al. (1986), Polar cap F patches: Structure and dynamics, *J. Geophys. Res.*, **91**, 12,121.
- Weimer, D. R. (1995), Models of high-latitude electric potentials derived with a least error fit of spherical harmonic coefficients, *J. Geophys. Res.*, **100**, 19,595.

K. Hosokawa and T. Kashimoto, Department of Information and Communication Engineering, University of Electro-Communications, Chofugaoka 1-5-1, Chofu, Tokyo 182-8585, Japan. (hosokawa@ice.uec.ac.jp; kashimoto@ice.uec.ac.jp)

T. Ogawa, National Institute of Information and Communications Technology, Nukui-Kitamachi 4-2-1, Koganei, Tokyo 184-8795, Japan. (taogawa@nict.go.jp)

Y. Otsuka and K. Shiokawa, Solar-Terrestrial Environment Laboratory, Nagoya University, Nagoya, Aichi, Japan Furo-cho, Chikusa-ku, Nagoya 464-8601, Japan. (otsuka@stelab.nagoya-u.ac.jp; shiokawa@stelab.nagoya-u.ac.jp)

S. Suzuki, Sugadaira Space Radio Observatory, University of Electro-Communications, Chofugaoka 1-5-1, Chofu, Tokyo 182-8585, Japan. (shin.s@ice.uec.ac.jp)